Nanoscale

Accepted Manuscript

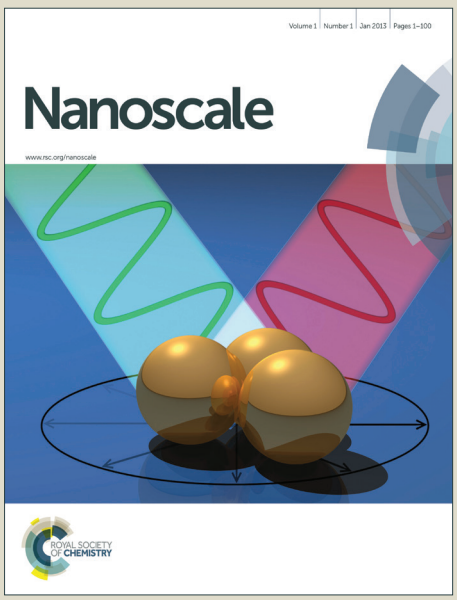

ROYAL SOCIETY OF CHEMISTRY

www.rsc.org/nanoscale

ARTICLE TYPE www. rsc.org/xxxxxx | XXXXXXXX

Artificially modified magnetic anisotropy in interconnected nanowire networks

Elsie Araujo,[a] Armando Encinas,[a] Yenni Velázquez-Galván,[a] Juan Manuel Martínez-Huerta,[b] Gaël Hamoir,[b] Etienne Ferain,[b,c] and Luc Piraux *[b]

Received Xth XXXXXXXXXX 20XX, Accepted Xth XXXXXXXXX 20XX
First published on the web Xth XXXXXXXXXX 200X
DOI: 10.1039/b000000x

Interconnected or crossed magnetic nanowire networks have been fabricated by electrodeposition into a polycarbonate template with crossed cylindrical nanopores oriented ± 30° with respect to the surface normal. Tailor-made nanoporous polymer membranes have been designed by performing a double energetic heavy ion irradiation with fixed incidence angles. The Ni and Ni/NiFe nanowire networks have been characterized by magnetometry as well as ferromagnetic resonance and compared with parallel nanowire arrays of the same diameter and density. The most interesting feature of these nanostructured materials is a significant reduction of the magnetic anisotropy when the external field is applied perpendicular and parallel to the plane of the sample. This effect is attributed to the relative orientation of the nanowire axes with the applied field. Moreover, the microwave transmission spectra of these nanowire networks display an asymmetric linewidth broadening, which may be interesting for the development of low-pass filters. Nanoporous templates made of well-defined nanochannel network constitute an interesting approach to fabricate materials with controlled anisotropy and microwave absorption properties that can be easily modified by adjusting the relative orientation of the nanochannels, pore sizes and material composition along the length of the nanowire.

1 Introduction

Over the last two decades, arrays magnetic nanowires (NWs) electrodeposited into nanoporous templates have received significant attention since they have many potential applications in magnetic and spintronic devices, sensors,[1] data storage,[2] microwave absorption,[3] magnetic-ferroelectric nanocomposites,[4] resistive switching memories[5,6] and magneto-optical properties.[7] A central problem regarding these NWs is to accurately control their magnetic properties in order to fine-tune their response to applied magnetic fields.

In a parallel nanowire array (PNWA) made of a single material, the magnetic properties can be changed varying different material parameters such as the NW diameter and height, the wire density, and the type of material. Furthermore, tuning of their magnetic properties can be done by adjusting electrodeposition conditions, such as bath temperature,[8] deposition potential,[9–11] electrolyte composition and pH value.[12]

There are several strategies to modify the NW arrays in order to produce materials that differ from the parallel array of homogeneous nanowires. One is done by modifying the composition of the NWs or by considering nanowires with axial/radial heterostructures. Examples include multilayered NWs,[13,14] core/shell nanowires,[15–17] bi-magnetic or bi-layer NWs such as growing two distinct materials or two different magnetic phases of the same material as reported recently for Co[18–20] and Ni NWs,[10] or even by using an alloy gradient along the growth direction.[21] A second strategy is to modify or condition how the deposition process takes place, for instance by using lithography to produce well defined areas of arbitrary shape with nanowires.[22] Another variation is to mask the template surface in successive stages to produce stair-like height profile NWs[23] or to use dip coating to produce NW arrays with a continuous height gradient profiles.[24] In all these cases, the NWs are both cylindrical and parallel; furthermore, these methods are independent of the targeted choice of the template since they can be implemented in nano porous anodic aluminium oxide (AAO) or track-etched polymer membranes.

Another option is based on the modification of the template itself to produce filamentary nanostructures with arbitrary aspect ratios and geometries that differ from the parallel cylindrical NW array. This has been recently exploited in AAO templates to produce diameter modulated NWs[25–31] which have led to materials with specific magnetic properties that differ from those in PNWAs.

The production of nanoporous particle track-etched polycarbonate (PC) membranes is based on a well-established technology operating at large scales to produce nanofiltration membranes. In this process, a thin polycarbonate film is irradi-

[a] *Instituto de Física, Universidad Autónoma de San Luis Potosí, Av. Manuel Nava 6, Zona Universitaria, 78290 San Luis Potosí, SLP, México.*
[b] *Institute of Condensed Matter and Nanosciences, Université Catholique de Louvain, Place Croix du Sud, B-1348, Louvain-la-Neuve, Belgium.*
[c] *it4ip s.a., avenue Jean-Etienne Lenoir, B-1348 Louvain-la-Neuve, Belgium.*

ated with energetic heavy ions that produce ion tracks within the polymer, followed by selective ion-track dissolution and formation of channels by chemical etching.[32,33] An interesting option to produce large area cylindrical nanowire arrays by electrodeposition that deviate from the usual PNWA, is to change the pore orientation with respect to the surface normal or, as shown recently by Rauber, et al.,[34] to perform sequential exposures of energetic heavy ions at different incidence angles to produce well-defined arrays of three dimensional interconnected cylindrical nanopores. In this manner, using two exposures will lead to crossed NW networks with bipod features, while three exposures will produce tripod type NW networks, etc.

In the present study we have prepared PC templates using a double energetic ion exposure to fabricate three-dimensional arrays of interconnected NWs made of Ni and Ni/NiFe that are compared with parallel NW arrays. The crossed nanowire array (CNWA) is shown to be self-standing after removal of the polycarbonate template. Their hysteresis loops measured by applying the external field in the out of plane (OOP) and in plane (IP) directions show a significant decrease of the magnetic anisotropy, which is interpreted in terms of the relative orientation of the NWs in the network. These results are further confirmed by the analysis of ferromagnetic resonance (FMR) measurements. Moreover, these NW networks exhibit an asymmetric broadening of the FMR line width, which is interesting for wide band microwave absorbing materials, in particular, low-pass filters. Finally, this approach provides a method to control the magnetic properties of the material by simply changing the energetic heavy ion beam incidence angle to set the relative orientation of the grown NWs.

2 Experimental

The crossed nanoporous templates have been prepared by performing a sequential two-step exposure of energetic heavy ions, done at a **30° and -30°** angle with respect to the normal of the PC membrane surface. The latent tracks generated by the heavy ions were chemically etched in **a 0.5 M NaOH aqueous solution at 70°C** to form nano pores, following previously reported protocol.[32] For the present study, the pore diameter is 230 nm and the membrane **surface** porosity is 20%, **a scaning electron microscope (SEM) micrograph of the resulting membrane surface is shown in Figure 1 (a)**. Additionally, a parallel pore template with the same pore diameter and porosity has been used. **As reported previously,[32] this method yields nanopores with a diameter dispersion of ± 5%. From these values, the average interpore distance on the surface of the membranes is calculated by averaging the interpore distances for a two dimensional hexagonal and square lattices, leading to an average distance of 473 nm. In the parallel pore template this distance is constant, while in the crossed nanopore template one cannot define an average interpore distance. However, there is an increase in the length of the pores related to their orientation that increases the volumetric porosity to 23%.**

Ni NWs have been grown by electrodeposition into the pores of regular (parallel) as well as crossed pore PC templates using a 262.84 g/l $NiSO_4$ + 30 g/l H_3BO_3 electrolyte, **having a pH=3.4,** with a constant potential of V = -1.1 V. Parallel and crossed bi-magnetic nanowires have also been prepared so that nominally 3/4 of the total wire length is made of Ni and the remaining 1/4 corresponds to a NiFe alloy which was deposited at a **constant** potential of V=-1.05 V using a 5.56 g/l $FeSO_4$ + 131.4 g/l $NiSO_4$ + 30 g/l H_3BO_3 electrolyte **with a pH of 3.0**. Prior to deposition, a 20 nm Cr / 1000 nm Au layer was evaporated on one side of the membranes to serve as a cathode. **All depositions where done at room temperature and the deposition times where between 800 and 1000 s.**

Characterization of the samples was done using scanning electron microscopy, alternating gradient magnetometry **with a maximum applied field of ±12 kOe** and ferromagnetic resonance. For the FMR measurements a microstrip line waveguide configuration has been used.[35] The 500 μm wide and 500 nm thick micro strip has been evaporated on the free surface of the PC membrane once the electrodeposition had been done. FMR measurements were performed at a constant frequency in the range of 100 MHz to 50 GHz, by sweeping the magnetic field applied **in the OOP direction** from 10 kOe down to zero field. All measurements in this study were done at room temperature.

3 Results and discussion

Figure 1 (b)-(d) shows SEM micrographs of the self-standing crossed Ni networks at different magnifications, while (e) shows the sample section used to perform the X-ray compositional analysis and (d) shows the corresponding compositional color scan image of the Ni/NiFe NWs. The PC membrane was dissolved using dichloromethane. As observed in the images, the continuous NWs fill the empty volumes of the membrane and produce a true replica of pores geometry. The NWs show homogeneous unions at the vertices, which form a 60° and 120° angles along the OOP and the IP direction, respectively. Finally, from the X-ray compositional image shown in Figure 1 (d) the different materials in the system can be identified: the Au from the electrode seen in purple, Ni in yellow and the NiFe alloy in green, which confirms the bi-magnetic nature of the nanowires. The vertical scale shows that the length of the Ni and NiFe segments have a relation close to 3/4 and 1/4, taking into account that the image is tilted.

Hysteresis loops have been measured in both parallel and

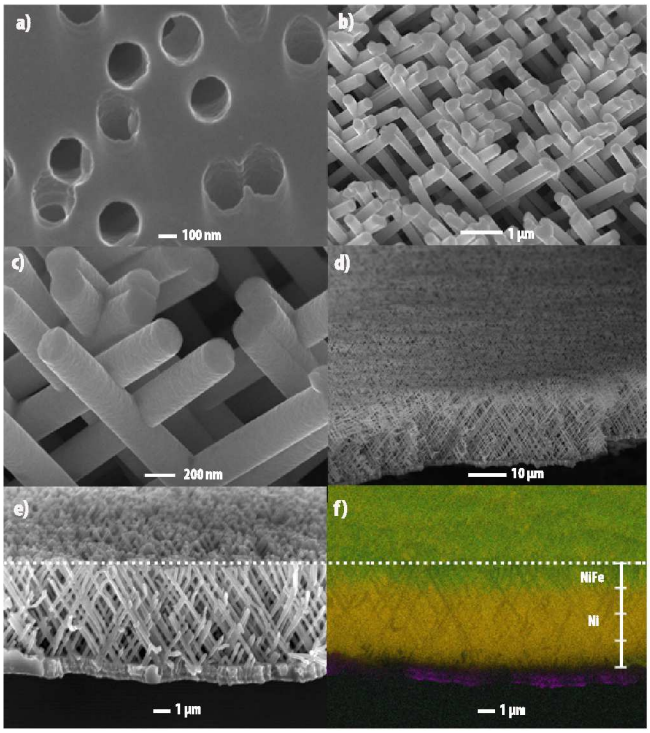

Fig. 1 SEM micrographs of (a) the surface of the double exposed polycarbonate porous membrane, (b)-(d) Ni-CNWA at different magnifications, (e) shows a side view of the section of the CNWA used to perform the X-ray compositional color scan image of the bi-magnetic Ni/NiFe CNWA, which is shown in (f) and where it is possible to distinguish the gold electrode (purple), the Ni (yellow) and the NiFe (green) segments. The dashed line is just for reference and gives the upper part of the nanowire network (tilted view).

crossed arrays of Ni and Ni/NiFe NWs with the field applied in the OOP and IP directions. Figure 2 shows the hysteresis loops measured in both directions for the case of (a) parallel Ni, (b) crossed Ni NWs, (c) parallel Ni/NiFe, and (d) crossed Ni/NiFe NWs. Additionally, Table 1 shows the values of the coercive field measured in both samples for each applied field direction. As expected, for parallel NWs, Fig. 2 (a) and (c) the hysteresis loops evidence the magnetic shape anisotropy characteristic of PNWAs, with an easy axis along the wire axis (OOP). The low remanence and coercivity observed in the OOP direction are related to the presence of magnetic domains, typical for such wire diameter and the demagnetizing effect of the interwire dipolar interaction. In contrast, for the CNWAs, Fig. 2 (b) and (d), a very significant reduction of the anisotropy is observed in both Ni and Ni/NiFe NWs.

As seen in the hysteresis loops of the crossed NWs, in the OOP direction the hysteresis loop stretches to higher field values while the opposite is observed in the IP direction. From

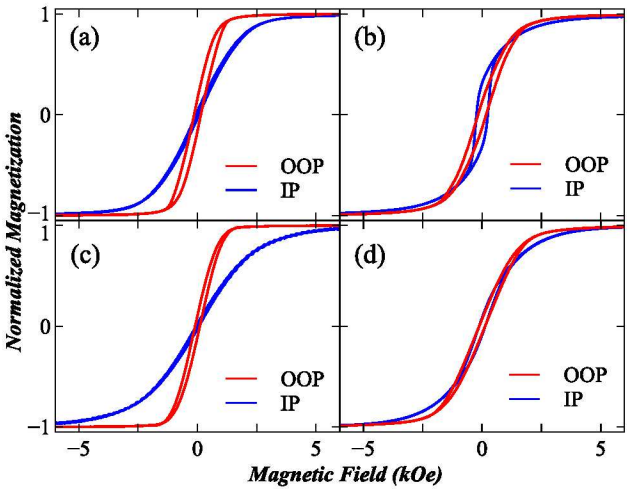

Fig. 2 Hysteresis loops measured with the external field applied out of the plane (OOP) and in the plane (IP) of the PC membrane in arrays of (a) parallel Ni, (b) crossed Ni NWs, (c) parallel Ni/NiFe, and (d) crossed Ni/NiFe NWs.

the values of the coercive field shown in Table 1, there is a clear increase of this field for CNWA in the IP direction with respect to the PNWAs. In the Ni CNWA the magnetization increases much faster in the IP than in the OOP direction. However, the system reaches the saturated state at lower field values in the OOP direction. A similar behavior is found in the Ni/NiFe CNWA shown in Fig. 2 (d).

Table 1 Values of the coercive field in parallel and crossed arrays of Ni and Ni/Fe NWs measured in the OOP and IP directions

Coercive field/(Oe)	OOP	IP
Ni-PNWA	144	65
Ni-CNWA	173	243
Ni/NiFe-PNWA	103	60
Ni/NiFe-CNWA	130	134

Comparing the results obtained in pure Ni and the bi-magnetic Ni/NiFe NWs, it is clear that the addition of a small quantity of the softer NiFe alloy results in changes of the magnetic properties. For example, a slight reduction of the coercive field in the PNWAs in the OOP direction is observed, H_c(Ni)=144 Oe and H_c(Ni/NiFe)=103 Oe. In the CNWAs similar changes are observed, in both OOP and IP directions, the coercive field is lower in the bi-magnetic NWs, as seen from the data in Table 1.

To interpret the effect of applying the external field in the OOP and IP directions in the CNWA, it follows from symmetry considerations that for the selected directions the field is actually applied with a certain angle with respect to the NWs axes. In particular, in the OOP configuration the NWs axes

are oriented at an effective angle that is equal to the angle at which the polycarbonate film was irradiated, in this case, $\pm 30^{\circ}$. While in the IP configuration the effective angle corresponds to the $\pm 90^{\circ}$ complement, in this case, $\pm 60^{\circ}$. These conditions will always be fulfilled when the high-energy ions incidence angle is the same in both exposures. In particular, if θ is the angle between the wire axis and the applied external field and $\pm\phi$ is the incidence angle of the energetic heavy ions, then the following relations hold for the OOP and IP configurations,

$$\theta_{OOP} = \phi \quad (1)$$

$$\theta_{IP} = \frac{\pi}{2} - \phi \quad (2)$$

As mentioned before, the changes in the hysteresis loops as well as in the magnetic anisotropy are related to the effective orientation of the NWs with respect to the external field when this is applied in the OOP or the IP directions. For both NiFe and Ni having a diameter of 230 nm it is reasonable to neglect any magnetocrystalline anisotropy contributions. In this sense, the observed reduction of the magnetic anisotropy is only related to the shape anisotropy and the dipolar interaction. Regarding the shape anisotropy, this will be reduced because the observed demagnetizing fields in the OOP and IP directions are both at intermediate angles with respect to the parallel and perpendicular directions of the wire axis. Comparing with the hysteresis loops measured on parallel NWs, in the OOP configuration the saturation field in crossed NWs are shifted to higher fields, while in the IP configuration they are shifted to lower field values, which suggests an increase (decrease) of the demagnetizing field in the OOP (IP) direction.

The other **contributions** to the effective anisotropy **are** the **exchange coupling arising at the junctions of the crossed nanowires** and the magnetostatic dipolar coupling that arises from the surface charge distributions generated when the NWs orient their magnetization in the direction of the applied field. **The exchange interaction at the junctions is not expected to result in a major effect since for both OOP and IP directions the magnetization is aligned with the applied field, provided that this field is strong enough, favoring the junction related exchange interaction, while at lower field values these junctions are more likely to act as preferential magnetic domain nucleation sites than to evolve towards less energetically favorable configurations. Whereas for the magnetostatic dipolar coupling,** the surface charge distribution obtained in CNWAs is very different and more complex that the one found in parallel NWs where this interaction is purely antiferromagnetic in the OOP direction or purely ferromagnetic when the field is applied in the IP direction. The effects of this interaction field cannot be assessed from the hysteresis loops, and other measurements are required.

In this sense, FMR measurements have been done on both parallel and crossed Ni and Ni/NiFe NWs with the external field applied in the OOP direction. FMR is a very powerful technique as it allows extracting precise values of the effective field from measurements done when the system is in the saturated state. Figure 3 compares the FMR spectra measured on

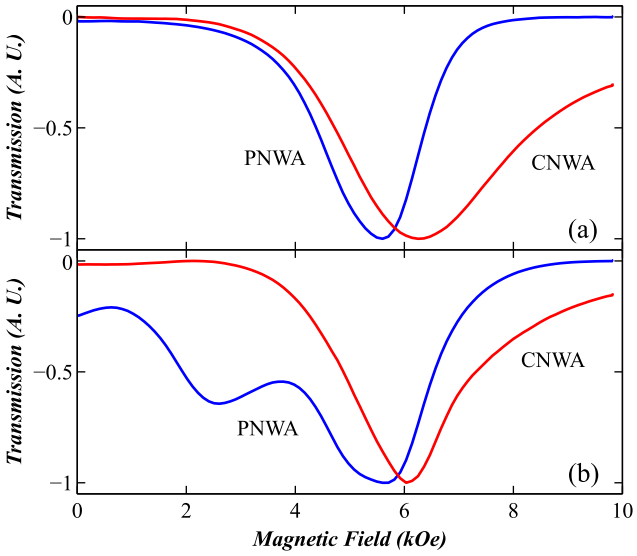

Fig. 3 Comparison of the FMR spectra measured on PNWA and CNWA at 21 GHz for (a) Ni, and (b) Ni/NiFe NWs.

PNWA and CNWA at 21 GHz for (a) Ni, and (b) Ni/NiFe. As seen in Fig. 3 (a) for the case of Ni NWs, the PNWA shows a typical FMR peak, whose minimum corresponds to the resonance field, while for the CNWA the minimum is shifted to a higher field value. Moreover, as observed by comparing both spectra, the FMR line width is significantly increased in the CNWA. In the case of the Ni/NiFe PNWA, Figure 3 (b), a more complex FMR line-shape is observed, in particular two absorption peaks are clearly visible that reflect the bi-magnetic composition of these NWs. The high field peak corresponds to the Ni segment in the NWs, which is larger than the NiFe segment and thus has greater amplitude FMR peak, and by comparison to the resonance field of the Ni PNWA shown in Fig. 3 (a). The lower field peak corresponds to the NiFe contribution since its smaller amplitude is consistent with a shorter segment length.

In contrast, for the Ni/NiFe CNWA a single, and large line width, FMR peak is observed; whose resonance field is very close to the Ni CNWA. The fact that a single peak is observed in the Ni/NiFe CNWA is attributed to the shift of the two peaks towards higher field values, and the presence of the NiFe segment results in a small contribution on the low field side of the peak which shifts the resulting resonance field to a value that is slightly lower than the peak of the pure Ni CNWA [Fig. 3 (a)].

By comparing the spectra measured on both CNWA it is seen that the FMR line width broadening is asymmetric with respect to the resonance field and the extra broadening of the resonance line takes place on the high field side. This feature, not observed in PNWAs, is potentially interesting for the application of these materials as low-pass microwave filters.

In order to obtain material parameters the FMR resonance condition for a purely magnetostatic array of parallel NWs has to be considered. This expression has been previously obtained using the Smit and Beljers formalism,[35,36]

$$\frac{f}{\gamma} = \Big[\big(H_{Ef}\cos 2\theta_0 + H_{Res}\cos(\theta_0-\theta_H)\big) \times \big(H_{Ef}\cos^2\theta_0 + H_{Res}\cos(\theta_0-\theta_H)\big) \Big]^{1/2} \quad (3)$$

where f is the excitation frequency, γ is the gyromagnetic ratio (3.09 GHz/kOe for Ni and 3.00 GHz/kOe for NiFe alloys[37]), H_{Ef} is the effective field, which contains the shape anisotropy and dipolar interaction contributions and H_{Res} is the resonance field. θ_0 is the angle of the saturated magnetization and θ_H is the angle of the applied field, both angles measured with respect to the easy axis that is taken as the surface normal.

For parallel NWs in the saturated state, $\theta_0 = \theta_H = 0$ and Eq. (3) reduces to the well know expression for PNWAs in the OOP configuration,

$$\frac{f}{\gamma} = H_{Ef} + H_{Res} \quad (4)$$

For the crossed NWs with the field applied in the OOP direction, it is assumed that they correspond to an array of NWs oriented at a 30° angle, in this case $\theta_0 = \theta_H = \pi/6$ and from Eq. (3) the resonance condition in the saturated state reduces to,

$$\frac{f}{\gamma} = \sqrt{\left(\frac{1}{2}H_{Ef} + H_{Res}\right) \times \left(\frac{3}{4}H_{Ef} + H_{Res}\right)} \quad (5)$$

For all the samples the dispersion relation has been constructed by measuring the resonance field from the spectra recorded at each different excitation frequency. Figure 4(a) shows the measured dispersion relation in the OOP direction for both Ni PNWA and CNWA. For PNWA Eq. (4) has been used to fit the data and an effective field of 1.2 kOe has been found. This value is in agreement with the theoretical value of 1.22 kOe for a Ni (M_s=485 emu/cm^3) PNWA with P=20%, which is calculated using $H_{Ef} = 2\pi M_s(1-3P)$.[35] **This result further supports that the magnetocrystalline anisotropy is indeed negligible and that the value of the average interpore distance of 473 nm in this PNWA is correct**. For comparison, the effective field for a low-density (P=0) array of Ni PNWAs is 3.05 kOe. For the CNWA, the corresponding dispersion relation is shifted downwards. As mentioned before, this decrease has been interpreted as a result of the average orientation of the crossed NWs when the external field is applied in the OOP direction. In this sense, the dispersion relation of the CNWA has been fitted using the expression for a PNWA when subject to a 30° applied field, Eq. (5). The corresponding fit is shown as a dashed line in Fig. 4 (a), from which an effective field of 0.9 kOe is found. This effective field is very close to the one found for the PNWA, which further supports the idea that CNWA behave as PNWA whose orientation correspond to the angle of the nanopores in the template. The small difference between the effective field values found in parallel and crossed NWs is attributed to the changes in the dipolar interaction field that, as mentioned before, is expected to be different in CNWA. To corroborate this, the dispersion relation given by Eq. (5) has been numerically calculated using the value of the effective field of 1.2 kOe determined previously for PNWA, the corresponding curve is shown as a continuous line. By comparing these dispersion relations, it is observed that the one for the CNWA falls below the one ex-

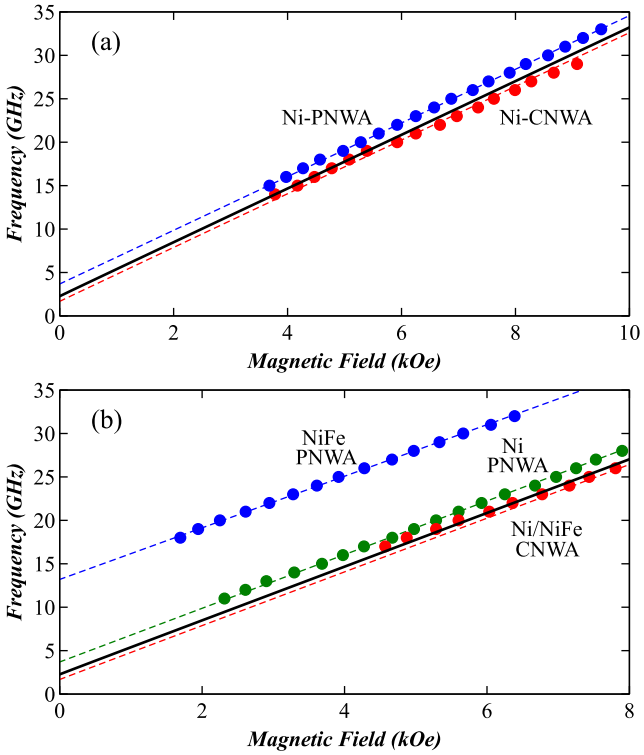

Fig. 4 Comparison of the dispersion relations measured in parallel and crossed arrays of (a) Ni, and (b) Ni/NiFe NWs. The dashed lines correspond to the fits to Eq. (4) for PNWAs and to Eq. (5) in the case of CNWAs. The continuous line corresponds to the dispersion relation calculated using Eq. (5) using the effective field of Ni PNWAs. It is noted that NiFe (Ni) PNWA corresponds to the low (high) field FMR peak shown in Fig.3 (b).

pected for PNWA, which suggests that the contribution of the **exchange and dipolar interactions** is stronger in CNWA.

The dispersion relations for the bi-magnetic Ni/NiFe PNWA and CNWA are presented in figure 4(b). As shown previously, Fig. 3 (b), the PNWA shows two distinct FMR peaks that have been attributed to the Ni and NiFe segments in the NWs, and the dispersion relation for each segment has been determined, as indicated in the figure. Equation (4) has been used to determine the effective field for Ni and NiFe. For the Ni segment, an effective field of 1.2 kOe is found, which is the same value found for the pure Ni PNWA (the difference is less than 50 Oe), while for the NiFe segment the effective field is 4.4 kOe, due to the higher saturation magnetization value of this alloy. For the Ni/NiFe CNWA where only one FMR peak is observed, Fig. 3 (b), the dispersion relation is shown along with the fit to Eq. (5) (dashed line) where an effective field of 1.34 kOe is found. This effective field is slightly larger than the one found in the Ni CNWA (1.2 kOe), which, as mentioned above, results from the small NiFe segment present in these wires.

Finally, the dispersion relation for a Ni PNWA subject to a 30° applied field has been calculated using Eq. (5) and the value of 1.2 kOe for the effective field previously determined for both the pure Ni and the Ni segment of the Ni/NiFe in PNWA, which is shown as a continuous line. A good agreement is observed between this result and those measured on the Ni/NiFe CNWA and similarly to the pure Ni case, the experimental points are shifted to lower values, which as mentioned above, it is attributed to the different dipolar interaction field values between parallel and crossed NW arrays. These results further support that the magnetic properties of these CNWAs are mostly determined by the orientation of the NWs with respect to the template's surface normal.

4 Conclusions

In summary, three-dimensional crossed nanowire networks display magnetic properties that differ significantly from the usual array of parallel-aligned NWs. The magnetic and microwave absorption properties of these ferromagnetic NW networks are found to be strongly dependent on the relative orientation of the NWs inside the polymer membrane. This orientation can be changed over a large range of values during the template fabrication so that it is possible to produce network NW arrays having different orientations. In this sense, the present results provide a promising venue for the fabrication of NW/polymer composites with tailored magnetic anisotropy and demagnetizing fields based on existing fabrication processes and employed for large-scale production of porous membranes.

Acknowledgements

This work was partly supported by CONACYT Mexico though grant CB-105568 as well as scholarships 328587 (E. Araujo), 348405 (Y. Velázquez-Galván) and postdoctoral fellowship 204131 (J. M. Martínez-Huerta).

References

1 B. Cox, D. Davis and N. Crews, *Sensors and Actuators A: Physical*, 2013, **203**, 335–340.
2 A. S. Samardak, E. V. Sukovatitsina, A. V. Ognev, L. A. Chebotkevich, R. Mahmoodi, S. M. Peighambari, M. G. Hosseini and F. Nasirpouri, *J. Phys.: Conf. Ser.*, 2012, **345**, 012011.
3 G. Hamoir, L. Piraux and I. Huynen, *IEEE Transactions on Magnetics*, 2013, **49**, 4261–4264.
4 L. Piraux, G. Hamoir, M.-W. Lee, E. Ferain, A. M. Jonas, I. Huynen and J. D. L. T. Medina, *Appl. Phys. Express*, 2011, **4**, 115001.
5 D. Ielmini, C. Cagli, F. Nardi and Y. Zhang, *J. Phys. D: Appl. Phys.*, 2013, **46**, 074006.
6 D. S. Jeong, R. Thomas, R. S. Katiyar, J. F. Scott, H. Kohlstedt, A. Petraru and C. S. Hwang, *Rep. Prog. Phys.*, 2012, **75**, 076502.
7 B. Toal, M. McMillen, A. Murphy, W. Hendren, R. Atkinson and R. Pollard, *Mater. Res. Express*, 2014, **1**, 015801.
8 K. M. Razeeb, F. M. F. Rhen and S. Roy, *Journal of Applied Physics*, 2009, **105**, 083922.
9 F. Tian, Z. P. Huang and L. Whitmore, *Phys. Chem. Chem. Phys.*, 2012, **14**, 8537–8541.
10 S. Dellis, A. Christoulaki, N. Spiliopoulos, D. L. Anastassopoulos and A. A. Vradis, *Journal of Applied Physics*, 2013, **114**, 164308.
11 A. Ramazani, M. A. Kashi and A. H. Montazer, *Journal of Applied Physics*, 2014, **115**, 113902.
12 M. Darques, A. Encinas, L. Vila and L. Piraux, *J. Phys. D: Appl. Phys.*, 2004, **37**, 1411.
13 J. De La Torre Medina, M. Darques, T. Blon, L. Piraux and A. Encinas, *Phys. Rev. B*, 2008, **77**, 014417.
14 Y. Su, J. Tang, H. Yang and Z. Cheng, *Nanoscale*, 2013, **5**, 9709.
15 Z. Liu, G. Xia, F. Zhu, S. Kim, N. Markovic, C.-L. Chien and P. C. Searson, *Journal of Applied Physics*, 2008, **103**, 064313.
16 T. N. Narayanan, M. M. Shaijumon, P. M. Ajayan and M. R. Anantharaman, *Nanoscale Res Lett*, 2010, **5**, 164–168.
17 D.-W. Shi, K. Javed, S. S. Ali, J.-Y. Chen, P.-S. Li, Y.-G. Zhaob and X.-F. Han, *Nanoscale*, 2014, **6**, 7215.
18 K. R. Pirota, F. Béron, D. Zanchet, T. C. R. Rocha, D. Navas, J. Torrejón, M. Vazquez and M. Knobel, *Journal of Applied Physics*, 2011, **109**, 083919.
19 P. D. Kulkarni, B. Sellarajan, M. Krishnan, H. C. Barshilia and P. Chowdhury, *Journal of Applied Physics*, 2013, **114**, 173905.
20 B. Sellarajan, P. D. Kulkarni, M. Krishnan, H. C. Barshilia and P. Chowdhury, *Applied Physics Letters*, 2013, **102**, 122401.
21 M. Zeng, H. Yang, J. Liu and R. Yu, *Journal of Applied Physics*, 2014, **115**, 17B514.
22 J.-M. Park, K. S. Nalwa, W. Leung, K. Constant, S. Chaudhary and K.-M. Ho, *Nanotechnology*, 2010, **21**, 215301.
23 J. D. L. T. Medina, J. Spiegel, M. Darques, L. Piraux and I. Huynen, *Applied Physics Letters*, 2010, **96**, 072508.
24 C. E. Carreón-González, J. De La Torre Medina, L. Piraux and A. Encinas, *Nano Lett.*, 2011, **11**, 2023–2027.
25 A. Rotaru, J.-H. Lim, D. Lenormand, A. Diaconu, J. B. Wiley, P. Postolache, A. Stancu and L. Spinu, *Phys. Rev. B*, 2011, **84**, 134431.
26 K. Pitzschel, J. Bachmann, S. Martens, J. M. Montero-Moreno, J. Kim-

ling, G. Meier, J. Escrig, K. Nielsch and D. Görlitz, *Journal of Applied Physics*, 2011, **109**, 033907.

27 G. D. Sulka, A. Brzózka and L. Liu, *Electrochimica Acta*, 2011, **56**, 4972–4979.

28 M. Raoufi and H. Schönherr, *RSC Adv.*, 2013, **3**, 13429–13436.

29 A. S. Esmaeily, M. Venkatesan, A. S. Razavian and J. M. D. Coey, *Journal of Applied Physics*, 2013, **113**, 17A327.

30 M. S. Salem, P. Sergelius, R. M. Corona, J. Escrig, D. Görlitz and K. Nielsch, *Nanoscale*, 2013, **5**, 3941–3947.

31 I. Minguez-Bacho, S. Rodriguez-López, M. Vázquez, M. Hernández-Vélez and K. Nielsch, *Nanotechnology*, 2014, **25**, 145301.

32 E. Ferain and R. Legras, *Nuclear Instruments and Methods in Physics Research Section B: Beam Interactions with Materials and Atoms*, 2003, **208**, 115–122.

33 M. E. Toimil-Molares, *Beilstein Journal of Nanotechnology*, 2012, **3**, 860–883.

34 M. Rauber, I. Alber, S. Müller, R. Neumann, O. Picht, C. Roth, A. Schökel, M. E. Toimil-Molares and W. Ensinger, *Nano Lett.*, 2011, **11**, 2304–2310.

35 A. Encinas-Oropesa, M. Demand, L. Piraux, I. Huynen and U. Ebels, *Phys. Rev. B*, 2001, **63**, 104415.

36 M. Demand, A. Encinas-Oropesa, S. Kenane, U. Ebels, I. Huynen and L. Piraux, *Journal of Magnetism and Magnetic Materials*, 2002, **249**, 228–233.

37 A. Encinas, M. Demand, L. Vila, L. Piraux and I. Huynen, *Applied Physics Letters*, 2002, **81**, 2032–2034.